Coupling Artificial Actin Cortices to Biofunctionalized Lipid Monolayers

Kheya Sengupta,*,†,§ Laurent Limozin,†,|| Matthias Tristl,† Ilka Haase,‡ Markus Fischer,‡ and Erich Sackmann†

Lehrstuhl für Biophysik, E22, Technische Universität München, James-Franck-Strasse 1, D-85748 Garching, Germany, and Lehrstuhl für Organische Chemie und Biochemie, Technische Universität München, Lichtenbergstrasse 4, D-85747 Garching, Germany

Received December 7, 2005. In Final Form: April 2, 2006

We report the assembly of protein supramolecular structures at an air−water interface and coupling of artificial actin cortices to such structures. The coupling strategies adopted include electrostatic binding of actin to monolayers doped with lipids, exposing positively charged poly(ethylene glycol) headgroups; binding of biotinylated actin to lipids carrying biotin headgroups through avidin; binding of actin to membranes through biotinylated hisactophilin (a cellular actin-membrane coupler) using an avidin−biotin linkage; and coupling of actin to membranes carrying chelating lipids through a 15-nm-diameter protein capsid (bacterial lumazine synthase or LuSy) exhibiting histidine tags (which bind both to actin and to the chelating lipid). The distribution of the proteins in a direction normal to the interface was measured by neutron reflectivity under different conditions of pH and ionic strength. In the case of the first three binding methods, the thickness of the actin film was found to correspond to a single actin filament. Multilayers of actin could be formed only by using the multifunctional LuSy couplers that exhibit 60 hexahistidine tags and can thus act as actin cross-linkers. The LuSy-mediated binding can be reversibly switched by pH variations.

Introduction

The actin cortex of the cell is a quasi-bidimensional assembly of actin filaments associated with the inner leaflet of the cell plasma membrane. The actin filaments are attached to the cell membrane through a variety of proteins or protein complexes that bind to actin on one hand and to the inner domain of membrane-penetrating proteins (such as cell surface receptors) on the other.[1] This versatile composite structure mediates important cellular functions and is responsible for the high mechanical stability of eukaryotic cells. Although many of the molecules involved in these composite shells have been identified,[2] the physical basis of their self-assembly and the relationships between their structural organization and their viscoelastic properties are still poorly understood. A recently developed strategy is the in vitro reconstruction of a biomimetic model of the membrane actin multilayer.[3−5] The design of in vitro models allows on one hand the use of various techniques of soft matter physics and on the other hand the definition of key components of self-assembly processes. For example, in vitro models have been successfully used to gain insight into cell locomotion[6] and cytoskeleton organization.[7]

A promising strategy for relating mechanical and viscoelastic properties of cell envelopes to the structure and membrane coupling of the actin cortex is the design of increasingly realistic models of cell envelopes and parallel studies of the structural and mechanical properties of cell envelopes and model systems. Membrane−actin composite shells have been designed by the self-assembly of actin shells on the outer surface of giant vesicles by membrane coupling through biotin−streptavidin−biotin linkers.[5] More realistic models were prepared by the self-assembly of actin cortices at the inner leaflet of giant vesicles by the polymerization of actin within giant vesicles.[3] Fuzzy actin shells were formed spontaneously in vesicles with radii smaller than the persistence length of actin. The driving force for self-assembly in this case was the minimization of the total bending energy of the composite shell. Thin actin cortices where formed by electrostatic coupling of actin filaments to positively charged membranes that were doped for this purpose with small amounts of lipids exposing positively charged macromolecular headgroups. These model systems are best suited to the evaluation of the mechanical and viscoelastic properties of composite shells by magnetic tweezers microrheometry.[3]

To study structural features, conformational dynamics, or the lateral diffusion of membrane-coupled actin filaments, planar models of the composite membrane shells are more appropriate because powerful surface-sensitive techniques can be applied to study these single-filament properties. These include microfluorescence, colloidal force spectroscopy,[8] and structural studies by neutron or X-ray surface scattering.[9−13] Of the two scattering techniques, even though X-ray offers better resolution, usually

* Corresponding author. E-mail: k.sengupta@fz-juelich.de.
† Lehrstuhl für Biophysik, Technische Universität München.
‡ Lehrstuhl für Organische Chemie und Biochemie, Technische Universität München.
§ Current address: Forschungszentrum Jülich, Leo-Brandt-Strasse, D-52428 Jülich, Germany.
|| Current address: Adhésion et Inflammation, CNRS UMR 6212, INSERM U600, Case 937-163 Av. de Luminy, 13288 Marseille Cedex 09, France.

(1) Janmey, P. A.; Xian, W.; Flanagan, L. A. *Chem. Phys. Lipids* **1999**, *101*, 93.
(2) Isenberg, G. *J. Muscle Res. Cell Motil.* **1991**, *12*, 136.
(3) Häckl, W.; Bärmann, M.; Sackmann, E. *Phys. Rev. Lett.* **1998**, *80*, 1786. Limozin, L.; Bärmann, M.; Sackmann, E. *Eur. Phys. J. E* **2003**, *10*, 319. Limozin, L.; Roth, A.; Sackmann, E. *Phys. Rev. Lett.* **2005**, *95*, 178101.
(4) Demé, B.; Hess, D.; Tristl, M.; Lay-Theng, Lee; Sackmann, E. *Eur. Phys. J. E* **2000**, *2*, 125.
(5) Helfer, E.; Harlepp, S.; Bourdieu, L.; Robert, J.; MacKintosh, F. C.; Chatenay, D. *Phys. Rev. Lett.* **2000**, *85*, 457.
(6) Loisel, T. P.; Boujemaa, R.; Pantaloni, D.; Carlier, M.-F. *Nature* **1999**, *401*, 613.
(7) Nedelec, F. J.; Surrey, T.; Maggs, A. C.; Leibler, S. *Nature* **1997**, *389*, 305.
(8) Dichtl, M.; Sackmann, E. *Proc. Natl. Acad. Sci. U.S.A.* **2002**, *99*, 6533.
(9) Miller, C. E.; Majewski, J.; Gog, T.; Kuhl, T. L. *Phys. Rev. Lett.* **2005**, *94*, 238104.
(10) Naumann, C.; Dietrich, C.; Behrisch, A.; Bayerl, T.; Schleicher, M.; Bucknall, D.; Sackmann, E. *Biophys. J.* **1996**, *71*, 811.
(11) Lösche, M. *Curr. Top. Membr.* **2002**, *52*, 117.
(12) Krueger, S. *Curr. Opin. Colloid Interface Sci.* **2001**, *6*, 111.

10.1021/la053310+ CCC: $33.50
Published on Web 05/25/2006

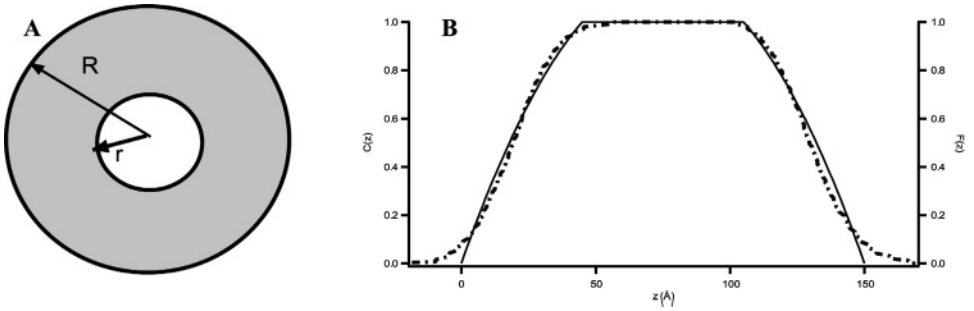

Figure 1. (A) Cross section of the hollow spherical LuSy. (B) Projected density profile of a layer of hollow spheres of outer radius 15 nm and inner radius 5 nm (−) and an example density profile generated for a homogeneous planar layer with a roughness factor (···).

neutron scattering is the technique of choice for probing functional proteins because, owing to its weaker interaction with the sample, it causes less radiation damage. Planar models of cell envelopes can be designed by the self-assembly of actin cortices on solid-supported membranes or on lipid monolayers at the air−water interface. Even though the former better mimics the bilayer nature of the cell membrane, the latter has the advantage of retaining in-plane lipid mobility even after the binding of multilayers of protein. Therefore, in the present work the second strategy was adopted in order to study the coarse-grained structure of membrane-coupled actin layers by neutron surface scattering.

We make use of newly synthesized coupling molecules to build various models of actin cortices and determine their structure by neutron reflectivity. This is a powerful method for studying the binding of proteins to biofunctionalized interfaces.[4,10−13] By injecting the required proteins step by step and collecting data after each binding step, it is possible to follow the gradual build up of multilayered systems. Because of the lack of any radiation damage, such titration experiments can be performed over long times to establish thermodynamic equilibrium that allows measurements of protein binding energies or Gibbs surface excess concentrations.[10] Neutron reflection provides the unique possibility of simultaneously measuring the layer thickness and the density of each protein layer.

We synthesized an icosahedral protein oligomer, the bacterial enzyme lumazine synthase (LuSy). It exhibits hexahistidine tags at each of its 60 monomers that bind nonspecifically to the actin filaments (in a pH-dependent manner) and specifically to the chelating group of the lipid anchors in the presence of Ni^{2+}. The binding can be reversed by EDTA. A specific feature of the LuSy coupler is that it provides a 15 nm spacer between the actin filament and the membrane, thus minimizing the nonspecific adsorption of actin to the surface by van der Waals attraction. We further tested several other simpler specific and nonspecific coupling schemes of actin filaments to phospholipid monolayers using more conventional molecules. These include (i) nonspecific electrostatic coupling of the highly negatively charged actin (7 positive excess charges per monomer) to monolayers containing lipid analogues with macromolecular headgroups exposing basic amino groups; (ii) specific coupling of biotin-exposing actin to lipids exhibiting biotinylated headgroups by avidin; (iii) coupling of actin to membranes exposing biotin−streptavidin linkers through the recombinantly prepared actin-membrane coupler hisactophilin (an actin binding protein from *Dictyostelia* cells) carrying a streptavidin-binding streptag peptide; and (iv) actin coupled to membranes exhibiting nickel-chelating groups via the multimeric, recombinantly prepared protein LuSy functionalized with hexahistidine tags. We compare the actin layer formed when membrane coupling is mediated by unspecific and reversible electrostatic binding or by more specific coupling. We demonstrate that the coupling of actin layers to the membrane through relatively short linkers (eg. biotin-streptavidin−biotin linkages) leads to the formation of single actin monolayers while multilayers are formed if the membrane coupling occurs through the multifunctional, giant coupler hexahistidine-tagged LuSy. Conversely, the density of the actin layer is strongly dependent on the mode of coupling and can be tuned by pH or salt concentration.

Materials and Methods

Description of Key Proteins and Lipids. The lumazine **s**ynthase molecule is a hollow icosahedral protein capsule with an outer diameter of 15 nm and an inner diameter of 5 nm (Figure 1).[14] It provides a versatile tool to biofunctionalize surfaces. Different functional groups can be coupled to its outer surface (in the present case a hexahistidine tag was attached to each monomer, leading to a total of 360 histidine groups on the surface), and it acts as a nanometric spacer that prevents the adsorption of proteins to solid surfaces by van der Waals attraction.[15] It was synthesized and decorated with the hexahistidine tags by the genetic recombination technique. (See Supporting Information for preparation details.) Here we shall focus on the binding of actin to the hexahistidine tags as a function of pH.

Hisactophilin is an actin binding protein found in *Dictyostelium* cells.[16] It was shown to be an essential protein for the osmoprotection of *Dictyostelium* cells.[17] It is a small, roughly cylindrical 13.5 kDa polypeptide that exhibits three histidine-rich loops on one face and a myristic acid chain on the other. It was established previously by neutron reflectivity and microfluorescence that the natural protein penetrates partially into the lipid monolayer and binds to actin through its positively charged histidine-rich motif.[10,18] Because the isoelectric point of histidine is pI ≈ 6.5, the binding of actin, which is negatively charged down to a pH of 5.6, can be switched by changing the pH of the system.[10] A genetic recombinant modification method was used to prepare a hisactophilin molecule exhibiting a strep-tag peptide (HISAC−streptag) that binds specifically to streptavidin or avidin. This peptide can be coupled to actin via the histidine-rich actin binding sites and to a monolayer of biotinylated lipids via the strep-tag. The latter binding is mediated by the protein streptavidin. (See Supporting Information for preparation details).

The phospholipids dimyristoylphosphatidylcholine (DMPC), dipalmitoylphosphoethanolamine-poly(ethylene glycol) 2000 amine (DPPE-PEG-amine or PEG-lipid), and 1,2-dioleoyl-*sn*-glycero-3-{[*N*-(5-amino-1-carboxypentyl)iminodiacetic acid]succinyl} (DOGS-NTA) were purchased from Avanti Polar Lipids. Biotin-X-DHPE lipids (*N*-((6-biotinoyl)amino)hexanoyl)-1,2-dihexadecanoyl-*sn*-glycero-3-phophoethanolamine) were purchased from Molecular Probes Inc. Avidin and streptavidin were purchased from Sigma-

(13) Kent, M. S.; Yim, H.; Sasaki, D. Y.; Satija, S.; Seo, Y.-S.; Majewski, J. *Langmuir* **2005**, *21*, 6815.
(14) Ritsert, K.; Huber, R.; Turk, D.; Landenstein, R.; Schmidt, B. K.; Bacher, A. *J. Mol. Biol.* **1995**, *253*, 151.
(15) Tristl, M. Doctoral Thesis, Technical University Munich, 2004.
(16) Scheel, J.; Ziegelbauer, K.; Kupke, T.; Humbel, B. M.; Noegel, A. A.; Gerisch, G.; Schleicher, M. *J. Biol. Chem.* **1989**, *264*, 2832.
(17) Pintsch, T.; Zischka, H.; Schuster, S. C. *BMC Biochem.* **2002**, *3*, 663.
(18) Hanakam, F.; Gerisch, G.; Lotz, S.; Alt, T.; Seelig, A. *Biochemistry* **1996**, *35*, 11036.

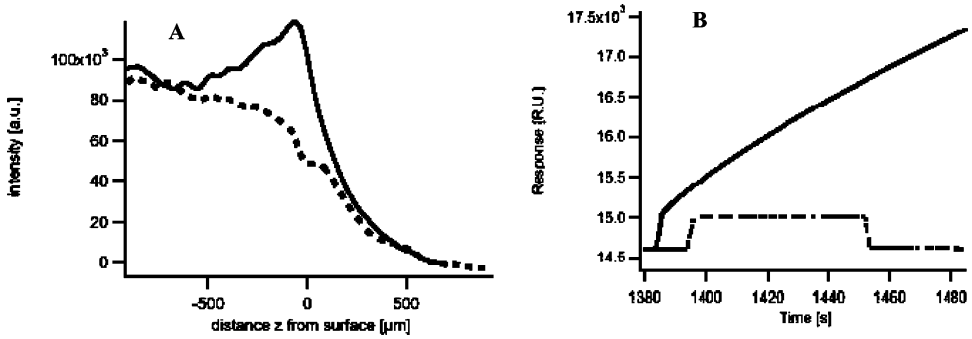

Figure 2. (A) Fluorescence intensity scans in a direction perpendicular to the interface immediately after (···) and 3 h after the injection of fluorescent histidine-Lusy (−). The sigmoidal dotted curve indicates that the fluorescent material is distributed in the bulk of the buffer whereas the peaked solid line clearly indicates an accumulation of material at the interface. (B) Surface plasmon resonance sensorgram showing the absorption of histidine-LuSy with and without preloading of nickel chelating molecules on the surface with Ni^{2+}. In the case of Ni^{2+} preloaded chelator complexes (−), the response shows an initial steplike response that corresponds to an increase in the refractive index of the histidine-LuSy solution. Next, a clear increase due to the binding of histidine-LuSy is visible. When the surface is pretreated with EDTA to deplete the chelator complexes of Ni^{2+} (···), the initial steplike response is again observed. However, when the injection of the protein-containing buffer is stopped, the response returns to the initial value, showing that no protein was bound.

Aldrich (Germany). Actin was prepared from rabbit muscle according to ref 20. (See ref 3 for a short description.) Biotin-labeled actin was prepared following the procedure of Okabe and Hirokawa.[20]

List of abbreviations that have been used extensively in the text is PEG-lipid or DPPE-PEG-amine, dipalmitoylphosphoethanolamine-poly (ethylene glycol) 2000 amine; biotin-X-DHPE, (*N*-((6-biotinoyl)amino)hexanoyl)-1,2-dihexadecanoyl-*sn*-glycero-3-phosphoethanolamine); HISAC-streptag, hisactophilin bearing one streptag; LuSy, lumazine synthase; histidine-LuSy, lumazine synthase capsids with each monomer coupled by genetic engineering to one hexahistidine tag.

Binding and Specificity of Histag-LuSy. To check whether histidine-LuSy does indeed bind to membranes containing chelator lipids in a selective way, we studied the binding of fluorescently labeled LuSy to monolayers of DMPC containing 10% Ni-NTA-DOGS. For this experiment, Texas red dye was covalently bound to LuSy in such a way that it was located in the enclosed cavity. The binding of the protein to the monolayer interface was tested by microfluorescence using the *z*-scan technique.[10] The fluorescence intensity was recorded while the objective of the microscope was moved in the vertical (*z*) direction. Figure 2A shows the fluorescence intensity distributions just after the protein was added to the buffer and the same after the passage of 3 h. Whereas initially the fluorescence intensity decays monotonically when the focus of the objective is moved from the subphase to the air, a sharp peak arises in the scan after 3 h, demonstrating that histidine-LuSy indeed binds to lipid layers containing chelating lipids. The specificity of binding of histidine-LuSy was demonstrated by the surface plasmon resonance technique using a Biacore Instrument (Biacore Inc., NJ) (Figure 2B).

Setup for Neutron Reflection. All of the neutron reflectivity experiments reported here were performed on the EROS time-of-flight instrument at the Orphée reactor (Laboratoire Léon Brillouin, Centre d'Etudes Nucléaires de Saclay, France[21]). A Teflon trough (volume 12 mL) enclosed in a temperature-controlled aluminum box with quartz windows was installed in the sample position. The surface pressure of the lipid monolayer was monitored by a Wilhelmy balance using a platinum plate. The incident angle was fixed at a low value (1.7° for the experiments with protonated LuSy, 0.87° for deuterated LuSy, and 1.9° for all others). The correct alignment of the instrument was ensured by collecting reflection data from a pure D_2O surface. In each scattering experiment, the spectra were collected during 0.5 or 1 h intervals, and the spectra from successive hours were compared to make sure that the binding process was complete. After the completion of the binding process, the successive runs were added to improve the statistics. Typically, for all proteins other than actin, 1 h was allowed for the binding of the protein followed by 2 h of exposure. In the case of actin, the exposure time ranged from 2 to 6 h.

Details of Sample Preparation. To maximize the contrast between the aqueous phase and the proteins (which were, with the exception of LuSy, available only in the protonated form), a subphase consisting of buffer prepared in pure D_2O was used. The trough was filled with measured quantities of the buffer. Appropriate amounts of lipids dissolved in chloroform were spread on the air−water interface by gently dropping the solution onto the buffer surface. Care was always taken to ensure that the surface pressure of the lipid layer was high enough (30 ± 5 mN/m) to prevent spontaneous accumulation of actin from the subphase onto the interface.[15,22] The proteins were injected through the monolayer using thin syringes in a stepwise fashion. We have confirmed, in separate experiments with fluorescently labeled lipids, that this process does not disrupt the structure of the monolayer. After each injection, sufficient time was allowed for the proteins to diffuse and bind to the interface and reach a steady state.

The buffer in each case was actin polymerizing F-buffer (2 mM Tris/HCl pH = 7.4, 1 mM ATP, 2 mM $MgCl_2$, and 0.2 mM dithiothreiol), and the sample chamber was thermostated at 25 °C. For some experiments, the pH was also set at 6 by the addition of HCl, and various concentrations of KCl (0, 150, 500, 750, and 1000 mM) were added. Actin was injected into the subphase in the form of monomeric globular actin (G-actin) to reach a final bulk concentration of 100 μg/mL. Under these conditions, actin is expected to polymerize in situ on the typical time scale of 30 min and absorb simultaneously to the various functionalized lipid or protein layers. In the following text, we describe the stepwise building of the four different multilayered structures studied. Figure 3A−D gives the scheme for each case.

(A) Actin bound unspecifically via the charged lipid DPPE-PEG-amine: A mixture of DMPC with 5% DPPE-PEG-amine was spread at the air−buffer interface, and monomeric G-actin was subsequently injected. The amine group at the end of the PEG chain is positively charged and is expected to bind actin (Figure 3A).

(B) Actin bound via the specific linker HISAC-streptag: A monolayer of biotin-X-DHPE was spread at the air−buffer interface.

(19) Fischer, M.; Bacher, A.; Haase, I.; Tristl, M.; Sackmann, E. *Chem. Phys. Chem.* **2001**, *10*, 623.

(20) Pardee, J. D.; Spudich, J. A. *Methods Enzymol.* **1982**, *85*, 154. Okabe S.; Hirokawa, N. *J. Cell Biol.* **1989**, *109*, 1581.

(21) http://www.llb.cea.fr/.

(22) The large uncertainty in the exact pressure of the lipid layer arose from the fact that the layer was spread to rather than compressed to the desired pressure. However, because in each of the experiments the actin was separated from the lipid layer either by the PEG−polymer moiety or by a layer of (avidin) streptavidin or by LuSy, the possibility of unspecific absorption of the protein at the air−water interface or directly onto the lipid monolayer was minimized (confirmed by negative tests). Because of this isolation, the exact pressure of the lipids was not expected to play a role in actin absorption.

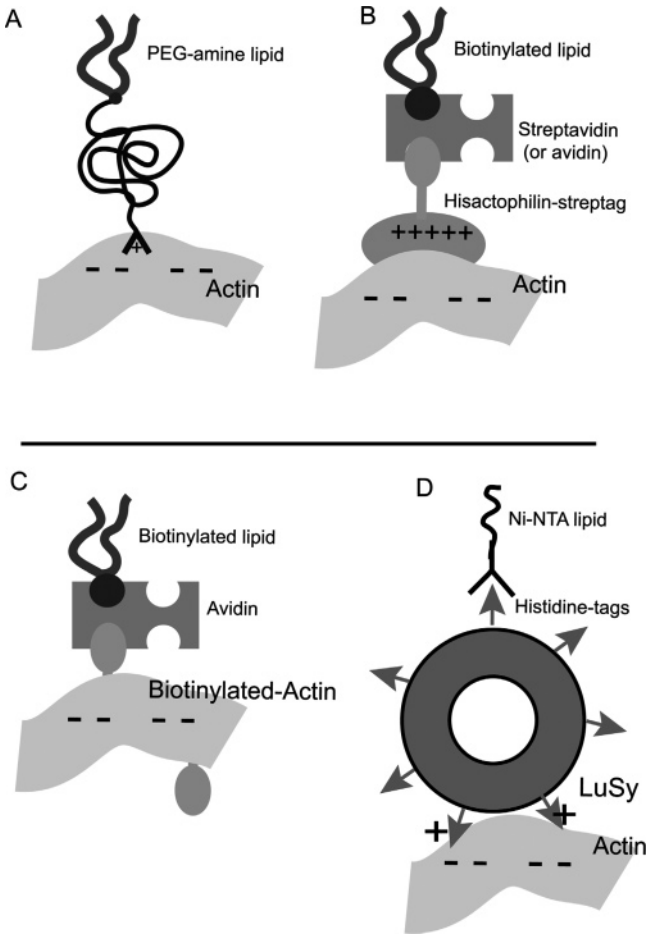

Figure 3. Schematic diagram (not to scale) of the protein multilayer assembly. (A) Actin bound to a lipid monolayer doped with DPPE-PEG-amine. (B) Actin bound to HISAC-streptag via streptavidin (or avidin) bound to a biotinylated lipid monolayer. (C) Biotinylated actin bound to avidin. (D) Actin bound to Ni-chelating lipids via histidine-LuSy.

The biotin binding protein streptavidin was injected ($c = 2\ \mu$g/mL) into the buffer in order to create a self-assembled monolayer of the protein under the lipid monolayer. Next, HISAC-streptag ($c = 2\ \mu$g/mL) was coupled to the monolayer functionalized with streptavidin. Finally, actin was injected (Figure 3B).

(C) Biotinylated actin bound via strong specific interaction: avidin−biotinylated actin. In this set of experiments, avidin (bulk concentration $c = 2\ \mu$g/mL) was bound to a DMPC monolayer containing biotin-X-DHPE. A mixture of pure and biotinylated G-actin was subsequently injected into the subphase. The biotin moiety of the actin binds specifically to the avidin. Two cases were considered: (i) monolayers of DMPC and biotin-X-DHPE in a 1:1 molar ratio with all of the actin monomers biotinylated and (ii) biotin-X-DHPE in a 9:1 molar ratio with 10% of the actin monomers biotinylated (Figure 3C).

(D) Actin bound reversibly via histidine-LuSy: A mixture of 90% DMPC and 10% nickel-NTA lipids was spread at the air−buffer interface. Histidine-LuSy was subsequently injected into the subphase (bulk concentration $c = 40\ \mu$g/mL) and bound to the lipids in a specific and reversible fashion. G-Actin was subsequently injected into the subphase containing polymerizing buffer (Figure 3D).

Neutron Reflection. The principle of neutron reflection has been explained in refs 23 and 24, and the application to lipid monolayers was described in ref 10. In brief, polychromatic neutrons are incident at a fixed angle θ, and all wavelengths greater than a critical wavelength exhibit total internal reflection. The wavelengths of the reflected neutrons are measured by the time of flight of particles between a chopper and the detector. The reflectivity $R(\lambda)$ of the interface is monitored as a function of the wavelength of the reflected neutron. In the present case, the successive layers of proteins were modeled as homogeneous layers (box model) with scattering length density ρ and thickness d. ρ and d are fitting parameters that are determined by fitting the reflectivity data against the theoretically calculated $R(\lambda)$, as will be explained in the following text. The reflectivity curves displayed here are expressed either as a function of wavelength λ or wavenumber k ($k = 2\pi \sin(\theta)/\lambda$). The data were typically fitted up to $k = 0.05$ Å^{-1}, which corresponds to a resolution (Δd) of 30 Å, taking the criterion $\Delta d \approx \pi/2k$. Note that this resolution is high enough to resolve a monolayer of actin ($d > \sim$60 Å).

Calculation of the Reflectivity Curve and Fitting Procedure. To calculate the experimental reflectivity curve, first the detector was exposed to the direct beam for several hours. The number of neutrons arriving at 128 separate channels of the detector, corresponding to 128 discrete wavelengths, was counted. Next the same procedure was repeated for the beam reflected from the sample. For each channel, the reflectivity is given by the total number of counted neutrons, divided by the number of neutrons counted in this channel from the direct beam. For each channel, a histogram of counted neutrons was constructed by sampling over time. The experimental error bar ($\epsilon_{data}(k_i)$) is the standard deviation of this histogram. This error scales as the inverse square root of the total exposure time.

The raw data ($R_{data}(k)$) was normalized in such a way that the plateau of total reflection corresponded to $R(k) = 1$. Next, the reflectivity curve expected for the chosen model with initial guessed values for the fitting parameters (R_{model}) was calculated following Demé et al.[4] The quantity $\chi^2 = \sum |R_{data}(k_i) - R_{model}(k_i)|/\epsilon_{data}(k_i)$ (where $\epsilon_{data}(k_i)$ are the errors) was calculated and minimized by varying the fitting parameters ρ and d.

Roughness. Often, in the literature, when a step function (box model) is used to describe a layered system, a roughness factor is introduced. A Gaussian of width σ at half-maximum is used to smooth the step functions describing the protein layers, and an overall roughness factor of $r = 2.5\sigma$ is defined for each layer. This roughness factor accounts for both the lateral heterogeneity of the individual layers and the smearing out of the steplike transition between two values of the scattering length density. In all the cases described here (with the exception of LuSy—see below), the converged value of the roughness (usually 0 to 3 Å) turned out to be much below the resolution of the system. This implied that changing the value of the roughness from zero did not change the χ^2 value significantly. Therefore, to reduce the number of fitting parameters, the roughness factor was ignored in the final fits reported here (with the exception of experiments with LuSy spacers).

Fitting Model for Histidine-LuSy. For the case of the histidine-LuSy protein, which has a hollow spherical shape (Figure 1), it was necessary to add a parameter representing the roughness of the interface between the histidine-LuSy layer and the adjacent layer representing the lipid or the aqueous phase. To a first approximation, the scattering length density of a homogeneously deuterated protein is proportional to its mass density. In the case of a hollow sphere of outer radius R and inner radius r, the mass density as a function of the vertical distance z is given by $\rho(z) = (R^2 - z^2)^{1/2}$ for $-R < z < -r$ and $\rho(z) = (R^2 - r^2)^{1/2}$ for $r < z < R$. Thus, the expected scattering length density for a monolayer of hollow spheres at an interface has the form shown by the solid line in Figure 1B. As shown by the dotted line in Figure 1B, this profile can be described by a model where the flat portion is taken as a homogeneous layer of uniform density separated from the air−water interface by a depletion layer, having a large roughness at both extremes.

Fitting of Multilayers. We exploited the fact that the protein layer was built step by step and data was collected after the addition of each new protein layer. Thus, in most cases (see discussion below for exceptions) there were only two fitting parameters: the thickness and scattering length density of one layer. The minimization was done using software written especially for analyzing reflectivity

(23) Russell, T. P. *Mater. Sci. Rep.* **1990**, *5*, 170.
(24) Penford, J.; Thomas, R. K. *J. Phys. Condens. Matter* **1990**, *2*, 1369.

data from the EROS reflectometer,[26] which uses the method of steepest descent. After the initial minimization, the initial guesses were varied to make sure that the converged values indeed corresponded to a global minimum. However, if the converged values seemed to be totally unphysical on the basis of our knowledge of the structure of the various proteins, they were rejected.

First, the data collected after the initial protein injection was fitted. The number of layers in the model was chosen to correspond to the number of lipid/protein layers expected. (Thus for the initial fit there were four parameters: the thickness and the densities of the lipid layer and those of the new protein layer. In case of the PEG-lipid, the first layer was fitted before the protein injection because in this case the PEG layer itself was the first layer.) For each additional layer bound, the fitting was done by keeping the parameters for the previous layers fixed at the converged value and fitting for the additional layer (two parameters). This was done once assuming that the new layer was indeed bound and once again assuming that the new layer was not present. This procedure ensures that the additional layer detected is not an artifact of the modeling. As before, the initial guesses for the parameters were varied to ensure that a global minimum had been reached, and the converged values were rejected if they violated our expectations based on physical grounds.

The major (but reasonable) assumption here is that the thickness and the scattering length density of the first layer do not change as a result of the binding of the second layer. In all cases, after following the above procedure, we additionally performed multiparameter fits (allowing more than two of the fitting parameters to vary) with different initial values to give ourselves a clear picture of the χ^2 terrain, to be sure that the converged values are indeed the best values, and to explore the nature of the interdependence of the various parameters. For example, through this procedure it emerged that the converged value of the thickness of the adjacent layers cannot be determined independently; χ^2 is sensitive only to the sum of the two thicknesses. However, because the thickness of the initially bound layer can be determined independently from the fit of the initial data set, the thickness of the next layer can be determined unambiguously.

Calculation of Surface Coverage and Errors. Following ref 4, the actin surface coverage was calculated as follows. The scattering length density of actin was taken to be $\rho_{actin} = 2.93 \times 10^{-6}$ Å^{-2} assuming that 79.5% of the labile hydrogens are exchanged by deuterium. The volume fraction Φ_{actin} of the actin in the layer is given by $\Phi_{actin} = (\rho_{buffer} - \rho_{layer})/(\rho_{buffer} - \rho_{actin})$ where ρ_{layer} and ρ_{buffer} are obtained from the fit of the data. The actin surface coverage (in units of weight/area) is then given by

$$\Gamma_{actin} = \Phi_{actin} m_{actin} d \quad (1)$$

where $m_{actin} = 1.38$ g/cm^3 is the mass density of actin and d is the thickness of the layer.

The total uncertainty in the estimation of the surface coverage ($\Delta\Gamma_{actin}$) has contributions from errors in both ρ and d and is given by $\Delta\Gamma_{actin} = [m_{actin}/(\rho_{buffer} - \rho_{actin})][(d\Delta\rho_{layer})^2 + ((\rho_{buffer} - \rho_{layer})\Delta d)^2]^{1/2}$, where $\Delta\rho_{layer}$ and Δd are the errors in ρ_{layer} and d, respectively. Conventionally, the error in the fitting is estimated by looking for a decrease of 10 to 15% in the χ^2 value.[10] However, in the case of nondeuterated proteins in deuterated buffer the error is expected to be dominated not by fitting but by the experimental statistical errors. Therefore, instead of taking the conventional criterion on χ^2, we develop an alternative criterion. First, the optimal fit is obtained by minimizing χ^2 as described before. Next, the parameter under consideration is manually varied around its optimal value, and χ^2 is again minimized by varying the other parameter while holding the parameter in question constant. For each new value of the parameters, the reflectivity curve is theoretically calculated and compared with the reflectivity curve calculated from the optimal fit (Figure 4). The parameter value is considered to be acceptable if the difference between the two reflectivity curves is smaller than the experimental error at each wavelength. The ensemble of acceptable values defines the uncertainty range of the parameter.

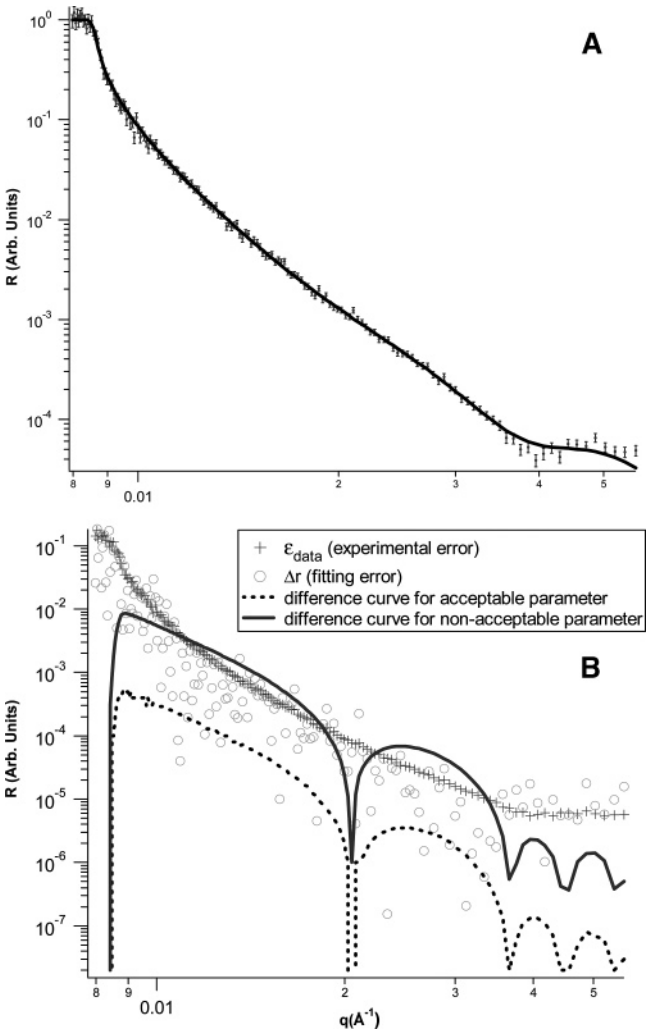

Figure 4. Typical reflectivity curve and corresponding error analysis in fitting parameter estimations. (A) Typical reflectivity curve for actin binding to HISAC-streptag at pH 6. The data points are shown with their error bars, and the fit is shown as a solid line. (B) Error analysis. For each channel (or wavelength), the value of the experimental statistical error (ϵ) given by the error bars was compared with the fitting error given by the difference between the experimental value and the fitted value $\Delta r = (|R_{expt} - R_{fit}|)$. The crosses correspond to ϵ, and the circles correspond to $|R_{expt} - R_{fit}|$. When the circles are below the crosses, the error is dominated by the experimental statistical error; otherwise, it is dominated by the errors in the fitting. Two examples of the difference in the reflectivity curves calculated from the optimal fit and from varying one of the fit parameters are also plotted. The dotted line, which is, at all wavelengths, below the experimental statistical error, corresponds to an acceptable value of the parameter whereas the solid line, which for some wavelengths is higher than the experimental statistical error, corresponds to an unacceptable value of the parameter.

Results

Structure of Histidine-LuSy. To evaluate the reflectivity plots, the LuSy layer was modeled as a homogeneous layer of uniform density, exhibiting a large roughness at both interfaces and separated from the lipid monolayer by a depletion layer. This model can account for the hollow quasi-spherical shape of histidine-LuSy as described above. The time evolution of reflectivity curves and density profiles of the absorbed layer is

(25) Born, M.; Wolf, E. *Principles of Optics*; Cambridge University Press: New York, 1999.

(26) Menelle, A. Private communication.

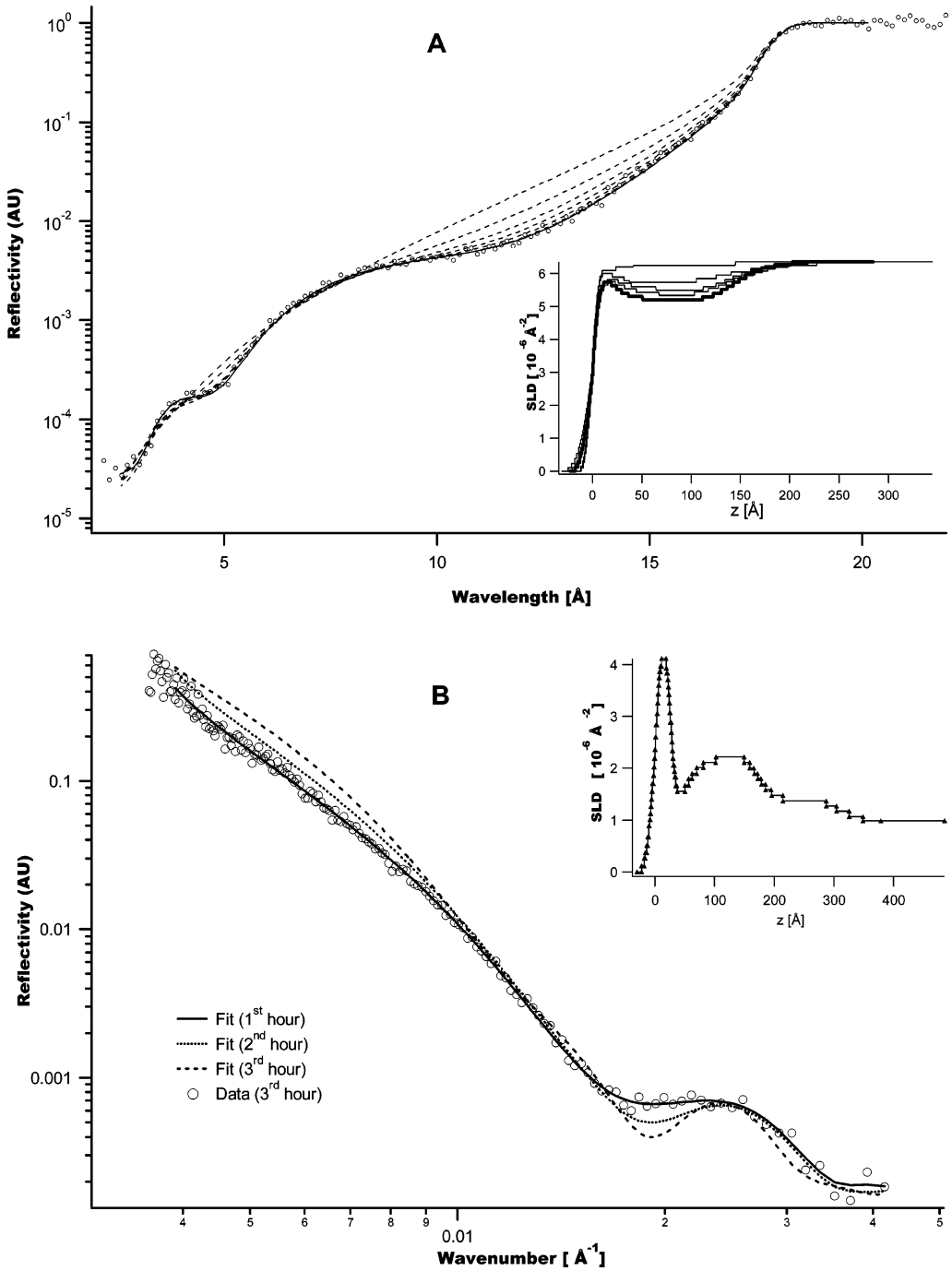

Figure 5. Reflectivity curves and corresponding scattering length density profiles of protonated (A) and deuterated (B) histidine-LuSy. (A) The symbols (○) represent experimental data points after 5 h of exposure, and the solid line is the corresponding fit. The dotted lines correspond to fits of data after 1, 2, 3, and 4 h (from top to bottom) of exposure. The inset shows the corresponding scattering length density profiles. (The earliest time corresponds to the topmost and the latest time corresponds to the bottommost profile.) (B) Symbols represent experimental data points after 3 h of exposure, and the solid line is the corresponding fit. The dashed and dotted lines correspond to data fits after 1 and 2 h, respectively. The inset shows the final scattering length density profile.

shown in Figure 5A. The final profile corresponds to a thickness of 12.2 nm and roughnesses of 0.5 nm at the lipid−protein interface and 1.5 nm at the protein−buffer interface.

To validate these parameters, we perfomed separate experiments with a deuterated version of histag-LuSy. In these experiments, the chelating lipids were dispersed in a matrix of deuterated DMPC. The buffer was prepared in a mixture of water (77.5%) and deuterium oxide (22.5%), which resulted in a scattering length density of about 10^{-6} Å^{-2}. The time evolution of reflectivity curves and the final density profile of the absorbed layer are shown in Figure 5B. In this case, the data from the 2nd and 3rd hours exhibits, in addition to the dense layer seen in the protonated case, an additional dilute layer of histidine-LuSy. The final profile for the dense layer corresponds to a thickness of 12.0 nm and roughnesses of 0.4 nm at the lipid−protein interface and 1.0 nm at the protein−buffer interface.

Binding of Actin. Typical examples of the scattering length density profiles for actin bound to lipid monolayers using the various schemes of Figure 3 are shown in Figure 6. The scattering length density (ρ) of air is always set to zero. In all cases, the first step of thickness $d \approx 10$ to 23 Å and $\rho \approx 2.7 \times 10^{-6}$ and 5×10^{-6} Å^{-2} corresponds to the lipid layer. The rest of the

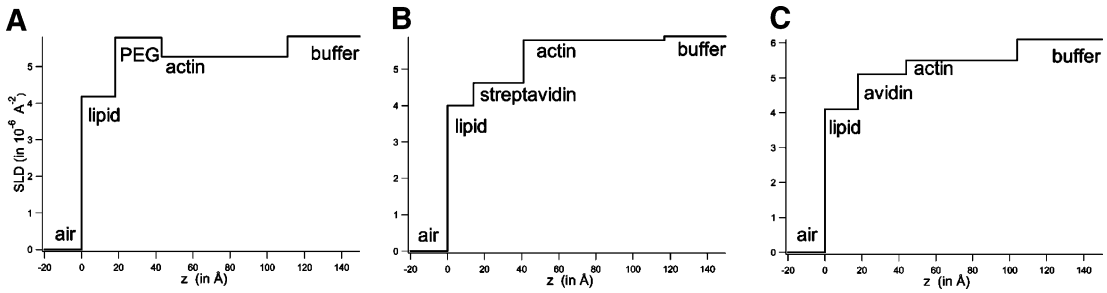

Figure 6. Scattering length density profiles of protein multilayers. (A) Actin bound to a lipid monolayer doped with DPPE-PEG-amine at pH 7 and ionic strength 500 mM. (B) Actin bound to HISAC-streptag via streptavidin bound to a biotinylated lipid monolayer at pH 6 and ionic strength 500 mM. (C) Biotinylated actin bound to avidin.

Table 1. Bacterial Strains, Plasmids, and Oligonucleotides Used in This Study

system	d(Å)	Γ(mg/m^2)
streptavidin/HISAC-streptag, no salt	71	1.01
streptavidin/HISAC-streptag, 150 mM salt	72	0.51
streptavidin/HISAC-streptag, 500 mM salt	76	0.35
streptavidin/HISAC-streptag, 1 M salt	59	0.68
avidin/HISAC-streptag, no salt	60	0.95
avidin/HISAC-streptag, 500 mM salt	50	0.47
avidin/biotinylated actin	57	1.4
(9:1 DMPC/biotin-DHPE, 10% biotinylated actin)		
avidin/biotinylated actin	55	2.0
(1:1 DMPC/biotin-DHPE, 100% biotinylated actin)		
DDPE-PEG-amine, no salt	71	1.9
DPPE-PEG-amine, 500 mM salt	68	1.79
DPPE-PEG-amine, 750 mM salt	86	0.19
DPPE-PEG-amine, 1 M salt	0	0
Histidine-LuSy	287	4.18

layers are system-specific and are described below. (See Table 1 for a summary of the results).

In the case of the nonspecific binding of actin via charged lipids DPPE-PEG-amine (Figure 3A) with no added KCl, the second step ($d = 43$ Å and to $\rho = 5.8 \times 10^{-6}$ Å^{-2}) corresponds to the PEG moiety of the lipid layer. The third step with $d = 68$ Å^{-2} and $\rho = 5.2 \times 10^{-6}$ Å^{-2} is negative (a reduction in ρ) and is determined by the actin whereas the final step ($\rho \approx 5.8 \times 10^{-6}$ A^{-2}) corresponds to the buffer. The experiment was performed at pH 7 for four different salt (KCl) concentrations (0, 500, 750, and 1000 mM). In each case, the DPPE-PEG-amine lipids were modeled as two-step functions, the first accounting for the lipid moieties ($\rho \approx 4 \times 10^{-6}$ to 5×10^{-6} Å^{-2} and $d \approx 11$ to 23 Å) and the other accounting for the PEG chains that dangle into the buffer from the lipid headgroups ($\rho \approx 5.6 \times 10^{-6}$ to 5.8×10^{-6} Å^{-2} and $d \approx 34$ to 43 Å). The scattering length density is close to the scattering length density of the buffer because the PEG is very dilute. The thickness of the PEG heads is in good agreement with ref 27, which reports a value of around 40 Å for 5% PEG-decorated lipids. Figure 7 shows typical examples of reflectivity curves, a comparison of the fit and data, and the variation of χ^2 close to a fitted minimum as a function of the actin layer thickness.

In the case of specific binding of actin using HISAC-streptag (Figure 3B), in the absence of added KCl, the second step corresponds to streptavidin ($d = 40$ Å and $\rho = 4.6 \times 10^{-6}$ Å^{-2}), the third to actin ($d = 76$ Å and a value of $\rho = 5 \times 10^{-6}$ Å^{-2}), and the final layer to the buffer ($\rho = 5.9 \times 10^{-6}$ Å^{-2}). The HISAC-streptag peptide, which is intercalated between the streptavidin and actin layers, could not be resolved as a separate entity after actin was bound. It was verified in a separate experiment that in the absence of HISAC-streptag, actin fails to bind to streptavidin. Experiments were performed either at pH 7 in the absence of any added KCl or at pH 6 with four different KCl concentrations (0, 150, 500, 1000 mM). In a separate set of experiments, the protein avidin was used instead of streptavidin. In this case, the pH was 6, and the KCl concentration was 0 or 500 mM. In each case, the streptavidin layer exhibited a ρ value between 4.6×10^{-6} and 4.8×10^{-6} Å^{-2} and a thickness between 34 and 44 Å (in agreement with the value of 43.7 Å in ref 10).

The surface coverage (Γ) and the thickness of the actin layer as a function of salt concentration for the two systems discussed above are shown in Figure 8. In the DPPE-PEG-amine case, up to a salt concentration of 500 mM, $\Gamma \approx 1.9$ mg/m^2 and $d \approx 70$ Å with a calculated uncertainty of about 9 Å. This thickness corresponds to the diameter of a single actin filament, leading to the conclusion that the actin cortex consists of a monolayer of filaments. At 750 mM salt, Γ is drastically reduced to about 0.2 mg/m^2 and d is about 86 Å with an uncertainty of 16 Å. At an even higher salt concentration of 1 M KCl, it is not possible to fit the data with a reasonable thickness for the actin layer. If it is assumed that a single actin layer is formed, then the optimal fit of the data yields a value of 17 Å for the thickness with an unreasonably high value of the uncertainty of 22 Å. We thus conclude that at such high salt concentrations the actin is not bound to the PEG amine chains at all. Actin also failed to bind to a monolayer consisting of 5% uncharged DPPE-PEG lipids in a DMPC matrix, showing that in this system there is very little nonspecific absorption in the absence of the charged DPPE-PEG-amine lipids.

In the steptavidin/HISAC-streptag case (Figure 3B), Γ ranges from 0.35 to 1.01 mg/m^2. The thickness varied between 50 and 76 Å, which is again consistent with the thickness of one actin filament. At pH 7 and in the absence of salt, we could not detect any bound actin. In the case where avidin was used instead of streptavidin, ρ and d were similar to those of streptavidin (4.6×10^{-6} Å^{-2} and 40 Å, respectively). This is expected considering the small structural differences between the two protein species. The HISAC-streptag could again not be resolved. The surface coverage of the bound actin layer was similar to the previous case and ranged from 0.5 to 1 mg/m^2, and the thickness was between 50 and 60 Å.

In the case of biotinylated actin bound to DMPC monolayers containing 10% biotinylated lipid via avidin (Figure 3C), the second step ($d = 44$ Å and $\rho = 5.1 \times 10^{-6}$ Å^{-2}) is again due to avidin. The third step corresponds to actin ($d = 57$ Å and $\rho = 5.5 \times 10^{-6}$ Å^{-2}), and the final step is determined by the buffer with $\rho = 6.1 \times 10^{-6}$ Å^2. Two cases were studied: (i) 9:1 DMPC/biotin-X-DHPE, 10% biotinylated monomers and (ii) 1:1 DMPC/biotin-X-DHPE, 100% biotinylated actin monomers. The parameters found for the lipid and the streptavidin layers agree well with the cases discussed above. For case i, the thickness of the actin was 57 Å (uncertainty range = 53 to 61 Å), and the

(27) Majewski, J.; Kuhl, T. L.; Gerstenberg, M. C.; Israelachvili, J. N.; Smith, G. S. *J. Phys. Chem. B* **1997**, *101*, 3122.

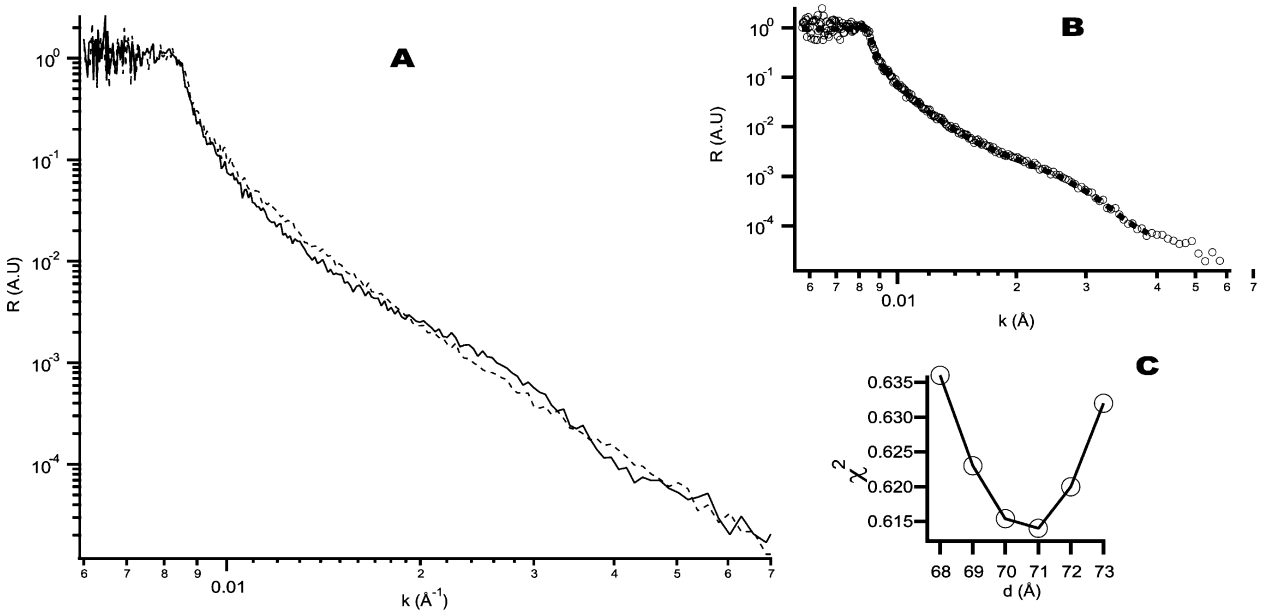

Figure 7. (A) Reflectivity curves of PEG + actin at no salt (−) and 1 M salt (- - -) concentration. (B) Fitted curve (- - -) and data (○) for the case of no salt where actin is supposed to have bound. (C) Variation of χ^2 around the fitted minimum as a function of the actin thickness.

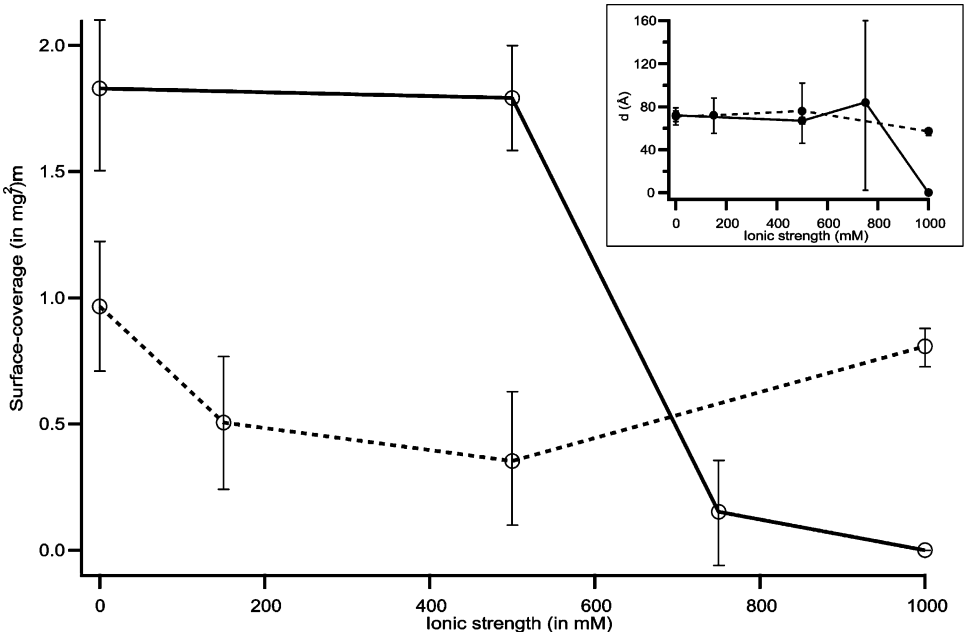

Figure 8. Surface coverage of actin as a function of salt concentration for coupling via PEG-amine groups (−) and HISAC-streptag (···). The inset shows the corresponding actin layer thicknesses. See the text for a discussion of the evaluation of the error bars.

surface coverage ranged from 1.3 to 1.5 mg/m^2. For case ii, the thickness was 55 Å (uncertainty range = 53 to 57 Å), and the surface coverage ranged from 1.9 to 2.1 mg/m^2. In both cases, the thickness of the actin is consistent with the absorption of one monolayer of filaments. The surface coverage in case i is denser than in the case of weak specific binding (steptavidine/HISAC-strep) but less dense than in the case of electrostatic binding (DPPE-PEG-amine). In case ii, the surface coverage is comparable to that achieved by electrostatic binding.

Binding of Actin to Histidine-Lusy. In the case of actin bound via histidine-LuSy at pH 6 (Figure 3D), the following structural data were obtained: for the lipids, $d = 20$ Å and $\rho = 4.2 \times 10^{-6}$ Å^{-2}, and for the LuSy layer $d = 101$ Å and $\rho = 5.0 \times 10^{-6}$ Å^{-2}. The interlayer roughness was $r = 10$ Å on the side facing the lipids and $r = 30$ Å on the side facing the actin. The actin layer was modeled as a homogeneous layer of $d = 290$ Å and $\rho = 5.64 \times 10^{-6}$ Å^{-2}. To obtain a reasonable fit, it was necessary to introduce a roughness of $r = 30$ Å for the actin layer as well. Note that the fitted layer thickness for LuSy decreased and the roughness increased after the binding of actin (Figure 9).

To establish the reversibility of actin binding, the initial pH of the buffer was kept at 7, and data were collected. Fitting this data showed that no detectable layer of actin was bound. Next the pH was lowered to 6 by injecting HCl dissolved in D_2O, and data was again collected. As discussed above, the fitting of this data clearly indicated a bound actin layer. The pH of the sample was then raised again to 7.8 by injecting KOH dissolved in D_2O, and data was collected. Fitting this data showed that the actin had become unbound from the histidine-LuSy.

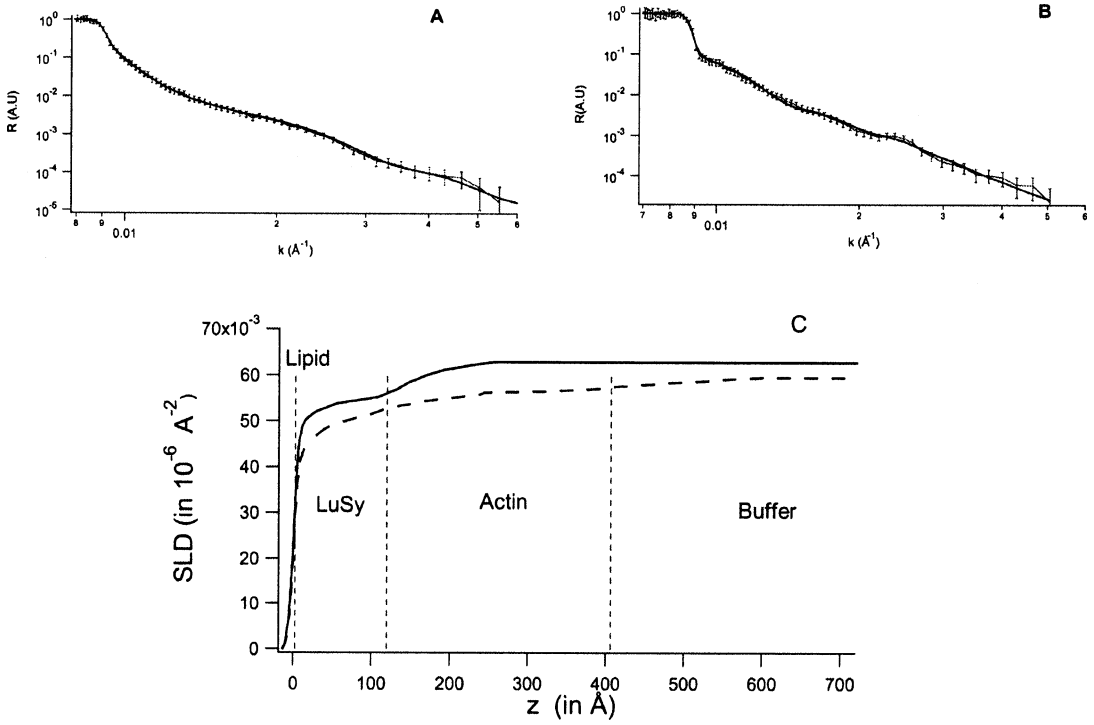

Figure 9. (A and B) Reflectivity curves of histidine-LuSy bound to Ni-chelating lipids at pH 6 before (A) and after (B) actin binding. (C) Corresponding scattering length density profiles: the dotted line is before and the solid line is after actin binding.

Concluding Discussion

In the present study, we introduced the use of the versatile linking protein LuSy in mimicking biological surfaces and explored different strategies to generate membrane-coupled 2D actin networks in order to design models of the actin cortex of cells. These networks can serve as models for further experiments, for example, to probe the mechanical properties of 2D actin networks in infinitely extended flat geometries. We showed that neutron reflectivity provides a useful tool for determining the surface density and the average thickness of the membrane-bound protein layers. Moreover it gives the opportunity of following the design of soft stratified films step by step.

The model systems studied were of varying degrees of complexity: The simplest case is that of charge-induced attraction. More complex schemes are based on the specific binding of actin to biotinylated membranes functionalized with streptavidin (or avidin) via actin molecules exposing biotin or by the natural actin-binding protein hisactophilin exhibiting ligands recognized by streptavidin. All three methods result in the formation of single monolayers of actin filaments, despite the fact that streptavidin is a multifunctional linker molecule. Actin shells consisting of cross-linked quasi-2D actin networks can be generated with the nanometric multifunctional LuSy linkers. This giant linker exhibits 60 ligands. The cross-linked semiflexible filaments are separated by distances of 15 nm, which facilitates the formation of relatively loosely packed networks. An advantage of this coupling scheme is its reversibility through changes in the pH by at most 1 unit.

The values of the layer thickness obtained by fitting the neutron reflectivity data agree well with structural data reported in the literature for the thickness of PEG chains, streptavidin (or avidin), and LuSy.[10,14,27] The parameters obtained for the lipid layers exhibit large variations probably because the surface pressure of the lipids could not be precisely controlled and measured but had to be adjusted by spreading appropriate amounts of lipids. Moreover, for the angles of operation accessible by the instrument, the sensitivity of the technique for the evaluation of the lipid structural parameters is inadequate, even though the actin, which is our primary interest, is still well resolved.

In the simplest case of electrostatic binding via the charged DPPE-PEG-amine lipids, the macromolecular chains act as spacers between the lipid monolayer and the actin whereas the positively charged amine groups dangling from the end of the chains bind the actin. A comparison with the case of actin binding to a monolayer of lipids exposing small positively charged headgroups, namely, DMTAP lipids in a DMPC matrix,[4] shows that in case of 100% or 10% DMTAP the surface coverage (2.5 mg/m^2) is considerably higher than the values found for DPPE-PEG-amine. In the case of 1% DMTAP, the surface coverage is 1.5 mg/m^2,[4] whereas in the presence of 1% DPPE-PEG-amine the coverage is 0.15 mg/m^2. The difference in the actin absorption for the same average surface charge density is probably due to an additional repulsive interaction of entropic origin exerted by the floppy PEG-amine chains.

The electrostatic binding of actin via DPPE-PEG-amine lipids was studied under four different ionic strengths of the buffer. For the case of no added salt and 500 mM KCl, a fairly dense (∼1.8 mg/m^2) layer of 70 Å thickness was found that is comparable to the diameter of one actin filament. At higher ionic strengths, the charges in the amine groups are expected to be screened, and actin is not expected to bind. Indeed, at an ionic strength of 750 mM, the surface coverage decreases to 0.2 mg/m^2, and the thickness increases to 86 Å. This is consistent with the case of actin binding to membranes containing charged lipids with small headgroups,[4] where an increase in the layer thickness with salt concentration is observed. At an ionic strength of 1 M, the actin fails to bind.

The natural pH-sensitive actin-binding protein hisactophilin was used to specifically bind actin to lipid monolayers. The hisactophilin itself was bound to the monolayer via the protein streptavidin or avidin. We found that hisactophilin does not bind significant amounts of actin at a pH where it loses its net positive charge (pH >7). However, unlike the case of charge-induced binding of actin (to DPPE-PEG-amine), the surface coverage of

actin does not show a systematic dependence on the ionic strength of the buffer and varies between about 0.35 and 1 mg/m^2. In each case, the thickness of the actin layer corresponds to the diameter of one actin filament. There is no systematic dependence of the layer thickness on the ionic strength. Avidin is positively charged at pH 6; therefore, even in the absence of any specific interaction, it binds actin simply because of electrostatic attraction. We found that the charge of the avidin layer does not lead to extra enrichment of the actin near the surface.

Each of the 60 hexa-histidine tags on the histidine-LuSy molecule consists of only six histidine groups as compared to 31 in hisactophilin. Despite this small size, it acts as an effective pH-sensitive actin coupler and can therefore mediate actin binding to membranes containing chelating lipids. However, it should be noted that there are 60 hexa-histidine tags on histidine-LuSy. Therefore, it is not proven conclusively in our experiments that a single hexa-histidine tag alone does bind actin. Because the histidine tag has an isoelectric point, pI, of 6.5, it can bind actin reversibly as a function of pH. The LuSy molecule decorated with 60 hexa-histidine tags thus provides an easy way to mediate the reversible coupling of the artificial actin cortex to the monolayer. The LuSy molecule acts as a versatile spacer because it can be modified by genetic engineering in many different ways. By reassembling protein oligomers exhibiting different functional groups (such as hisactophilin and biotin), one can generate linkers with mixed functionality. Another advantage of LuSy couplers is their large size. At a distance of 15 nm, intermolecular interactions are already weakened considerably, thus reducing the attraction (and therefore the nonspecific binding) of large protein assemblies (such as actin filaments) to solid surfaces. Moreover, the hollow interior of LuSy can be filled with a fluorescent dye, thus rendering the actin binding centers visible.

In conclusion, we have demonstrated a few different strategies for varying complexity and biomimicry to couple actin to a lipid layer. We find that the presence of large cross linkers, namely, the genetically modified and biofunctionalized 15 nm protein histidine-LuSy, is necessary for the formation of thick actin layers that, like the actin cortex of living cells, comprise multi- rather than monolayers. Our preliminary observations indicate that in the presence of biologically relevant actin binding proteins such as filamin, actin forms more complicated structures at the lipid interface that cannot be modeled by the simple box models presented here. The present experiments provide the means to couple actin to a lipid interface in a controlled manner and offer further insight into the organization of actin at such interfaces. These experiments should form the basis of further investigation into the details of the structural organization of actin at lipid interfaces in the presence of other more biologically relevant coupling proteins.

Supporting Information Available: Details of the preparation of the genetically engineered proteins histidine-LuSy and HISAC-streptag. This material is available free of charge via the Internet at http://pubs.acs.org.

Acknowledgment. We thank Dr. Alain Menelle for extensive help with the neutron setup and data analysis, Dr. Michael Baermann for biochemical advice, and Monika Rusp for the preparation of actin. We thank Sebastian Schwamb and Thomas Wojtulewicz for skillful technical assistance. This work was supported by the Deutsche Forschungsgemeinschaft (SFB 413, C3), by the Fonds der Chemischen Industrie, and by the VW Stiftung. K.S. and L.L. acknowledge a fellowship from the Humboldt Foundation.

LA053310+